

INVESTIGATION OF A SUBMERGED NOZZLE ON A 1/14.2-SCALE
MODEL OF THE 260-INCH SOLID ROCKET

By Reino J. Salmi and James J. Pelouch, Jr.

Lewis Research Center
Cleveland, Ohio

NATIONAL AERONAUTICS AND SPACE ADMINISTRATION

INVESTIGATION OF A SUBMERGED NOZZLE ON A 1/14.2-SCALE

MODEL OF THE 260-INCH SOLID ROCKET

by Reino J. Salmi and James J. Pelouch, Jr.

Lewis Research Center

SUMMARY

An experimental investigation of the flow characteristics about a submerged nozzle for the 260-inch solid rocket was conducted at the Lewis Research Center with a 1/14.2-scale model which used compressed air to simulate the exhaust gases. The study was concerned with induced flows and distortions that could result from the asymmetric cloverleaf-shaped grain port.

The results showed that low pressures due to separated flow at the aft ends of the propellant grain lobes induced a highly turbulent circumferential flow in the annular passage formed by the submerged nozzle lip and the aft-end rocket casing. In the actual rocket, such a flow in the annular passage could rapidly erode insulation filler materials not designed for use in areas subjected both to high temperatures and velocities. The separated flow region behind the grain lobes also distorted the circumferential Mach number distribution of the flow through the nozzle. Modifying the ends of the grain lobes from a flat surface to a wedge shape slightly reduced the induced flow velocities. Tests with a simulated 34 percent regressed grain, however, indicated that the induced velocities were diminished to the point where little or no adverse effects should occur.

INTRODUCTION

A partially submerged nozzle design has been proposed for the 260-inch solid rocket to provide the feasibility of developing a gimbaling nozzle. The new design also provides a shorter overall nozzle section for the solid rocket. The submerged nozzle is attached externally to the aft-end rocket casing at the minimum nozzle cross-sectional area and the nozzle entrance region protrudes into the rocket very near to the propellant grain.

Concern for the structural integrity of the new nozzle design, due to the high temperature and pressure environment, prompted a small-scale investigation of the gas flow

patterns in the region of the nozzle entrance lip. Of particular concern was the possibility of high velocity exhaust gas flow circulation in the annular passage formed by the nozzle lip and the aft-end rocket casing. The flow in the annular passage could be induced by asymmetric exhaust gas flows because of the cloverleaf-shaped grain port. The original design thickness of the rubber filler material in this area would be insufficient in the presence of high velocity, high temperature gases.

The tests were made in the Lewis Propulsion Systems Laboratory with a 1/14.2-scale model using compressed air to simulate the exhaust gases. Because the conical divergent section of the submerged nozzle was not required, the nozzle was cut off just downstream of the throat to simplify installation and instrumentation. The model was operated at a nominal chamber pressure of 20 pounds per square inch absolute (137 895 N/sq m), and the altitude facility was operated at approximately 2 pounds per square inch absolute (13 790 N/sq m). The flow patterns in the annular passage were studied by observing tuft behavior through a transparent aft-end casing. Mach number distribution in the annular channel and in the nozzle was determined from measurements of the static and total pressures.

APPARATUS

A 1/14.2-scale model of the Aerojet General 260-inch-diameter solid rocket motor, used in the tests of reference 1, was modified to simulate a submerged nozzle design. The model was tested in altitude test cell 2 of the Lewis Propulsion Systems Laboratory, which provided a sufficient weight flow of compressed air to choke the 30.6-square-inch (0.01974-sq m) nozzle throat at a chamber pressure of 20 pounds per square inch absolute (137 895 N/sq m) in the altitude environment. Figure 1 shows the model mounted in the test cell.

Since the divergent conical section of the submerged nozzle was not required for the tests, the nozzle was extended only 3/4 inch (0.019 m) downstream of the throat. The submerged nozzle and the transparent plastic aft-end casing, which was employed to allow visual observation of tuft behavior in the annular channel formed by the aft-end casing and the nozzle lip, are shown in figure 2, along with the perforated grain and the outer shell, which comprise the major components of the model. Figures 3 and 4 are photographs of the nozzle and transparent plastic casing; in each case, the side facing the annular passage between the nozzle lip and the casing is shown. These photographs also show the wool tufts attached to the surfaces forming the annular channel. The back side of the nozzle lip was painted white to improve contrast in the region where the wool tufts were attached. Black tufts were used on the white lip wall and red tufts were fastened to the transparent casing.

The internal grain contour for the model was fabricated from perforated sheet steel through which air flowed to simulate the emanation of exhaust gases from a burning propellant grain. The holes in the perforated grain were designed to be choked to keep the air weight flow uniform. The compressed air was supplied to an opening in the outer shell of the model by a 6-inch-diameter (0.1524-m-diam.) pipe. To determine the effects of grain-lobe end design on the flow in the annular channel, various modifications (configurations A to C) were made to the ends of the propellant grain lobes as shown in figure 5. Figure 6 presents a photograph of configuration A wherein the flat grain-lobe ends are sloped 30° (0.594 rad) from a plane normal to the grain centerline. Configuration D, which simulated a 34 percent regressed propellant grain, did not have a perforated surface; the air entered the combustion chamber from three holes located near the head end of the grain, as shown in figure 7.

Grain configurations A and B had solid surfaces at the grain ends. To determine the validity of the results obtained with the solid grain end, configuration C (which was identical to configuration B) was provided with uniform air bleed grain end proportional to its surface area relative to the grain surface area.

Multitube tetrabromoethane manometers along with mercury manometers were used to measure the total and static pressures. The locations of the static and total pressure instrumentation are presented in figure 8. The nozzle coordinates given in figure 8 define a nozzle lip shape which was slightly greater in diameter at the bottom of the lip than the actual design for the 260-inch rocket. However, this difference in nozzle diameter should have negligible effect on the results.

PROCEDURE

The tests were performed in the Propulsion Systems Laboratory altitude chamber with the solid rocket model operating at a nominal combustion chamber pressure of 20 pounds per square inch absolute (137 895 N/sq m) and the test chamber altitude pressure set at 2 pounds per square inch absolute (13 790 N/sq m). High-speed color movies of the tuft behavior were made through the transparent casing end to provide visualization of the flow in the annular passage between the nozzle lip and the aft-end rocket casing wall.

Since the nozzle was instrumented with only one row of static orifices, the pressures at various circumferential stations relative to the grain lobe, were obtained by rotating the submerged nozzle to a different position relative to the grain for each run. Total pressures in the annular passage were measured with a probe that could be remotely rotated. By referencing a radial line through the center of a grain lobe as zero, pressure measurements were made at various angles between 0 and 60° (1.046 rad), where

60° (1.046 rad) represents a radial line bisecting the angle between the grain lobes. Permanent records of the pressure data were obtained by photographing the manometer boards.

RESULTS AND DISCUSSION

Of primary interest in the investigation was the determination of the flow characteristics in the annular channel formed by the nozzle lip and the aft-end casing. The flow is defined by its direction and Mach number in the annular channel as presented in figures 9 and 10. These figures include photographs of the tuft behavior enlarged from single frames of the high-speed movies and Mach number contours computed from the measured pressures.

The tuft study movies indicated a very turbulent circulation of the simulated exhaust gases in the annular channel. The flow entered the channel from the trough between the grain lobes, which extended lower than the nozzle lip, and exited in the region directly behind the grain lobes as shown by the arrows in the sketch in figure 11. This circulation pattern was induced by a low base pressure region at the ends of the grain lobes, because of separation of the grain port exhaust flow. The high-speed tuft study movies indicated full channel flow in the annular passage by the similar behavior of the black and red tufts which were used to differentiate between the lip wall undersurface and the transparent aft-end casing wall.

To determine the effect on the channel flow resulting from modifications to the aft-end of the grain lobes, a wedge-shaped (configuration B, fig. 5) grain end was tested. The tuft studies showed that the modification had no effect on the turbulence and direction of the flow in the annular passage. Mach number contours of the flow in the annular channel (fig. 10) indicated that the highest velocities occurred in the region directly behind the grain lobes where the flow exited from the passage. The highest Mach numbers were obtained with configuration A, which had flat grain lobe ends. The velocities were only slightly reduced by the wedge modification.

A 34 percent regressed grain configuration (D) was tested to obtain an indication of the reduction in flow velocity in the annular passage that might occur as a result of increased port area and smaller grain lobes because of the burning of the propellant grain. The results showed that the general flow pattern in the annular channel was still evident, but that the Mach number level was greatly reduced. Although the regressed grain was not perforated, it is believed the results would not be appreciably affected.

Unsymmetrical nozzle flows can cause various adverse effects such as a reduction in the flow coefficient, nonuniform ablation and unsymmetrical nozzle forces. The asymmetry in the submerged nozzle flow due to the separated flow regions from the

grain lobes is shown in figures 12 to 14.

Figure 12, which shows the nozzle Mach number variation with area ratio for circumferential nozzle stations directly behind the grain lobes and midway between the grain lobes on the forward surface of the nozzle, indicated that, in general, substantially lower Mach numbers occurred for the station directly behind the grain lobes. The lower Mach numbers can be attributed to an extension into the nozzle of the wake from the ends of the grain lobes. However, at the low Mach number (high area ratio) region at the end of the nozzle lip, the flow exiting from the annular channel caused locally higher Mach numbers for the station directly behind the grain lobes.

Modifying the grain lobe end design from a flat surface to a wedge shape alleviated, to some degree, the reduction in nozzle Mach number by the grain lobe wake as shown in figure 12.

Since the asymmetric nozzle flows and annular channel flow are caused by the low pressure region at the ends of the propellant grain lobes, it was thought that the emanation of hot gases from the grain end might tend to alleviate the low pressures for the actual solid rockets. To establish the validity of the data obtained with the solid grain ends, the end of the grain lobe for configuration C, which has the wedge shape, was perforated with bleed holes and an amount of air proportional to its percentage of the grain surface area was bled from the perforated grain end. The effect of the grain end bleed was almost negligible, however, as shown by figure 13.

The circumferential Mach number variation in the nozzle is shown in figure 14 for two longitudinal stations in the nozzle. At orifice station 1, which was nearest the nozzle throat, configurations A, B, and C exhibited a nearly uniform increase in Mach number with the angle, α , which varied from 0 (directly behind the grain lobe) to 60° (1.046 rad) (midway between lobes). The circumferential Mach number variation at this station varied from about 0.13 for configuration A to 0.06 for configuration B. This reduction in the circumferential Mach number variation is the major benefit derived from the wedge-shaped grain ends. At station 3, which is at a larger area ratio, the Mach number tended to stay low in the area behind the grain lobe and then increase more rapidly to the value midway between the lobes. The 34 percent regressed grain (configuration D) exhibited virtually no circumferential distortion of the nozzle flow at either station.

CONCLUDING REMARKS

The results of an investigation of the flow characteristics about the entrance region of a submerged nozzle design proposed for the 260-inch solid rocket, indicated that undesirable induced flows and nozzle flow distortions could be attributed to the asymmetric grain port design. A low pressure separated flow region existed at the ends of

the grain lobes formed by the cloverleaf-shaped grain port. The low pressure region induced a highly turbulent circumferential flow in the annular channel formed by the nozzle lip and the aft-end rocket casing. In the actual rocket, this flow, which exhibited Mach numbers up to 0.2, could cause rapid erosion of insulation filler compounds not designed for high velocity, high temperature applications. A wedge-shaped modification to the grain lobe ends was relatively ineffective in reducing the induced flows. A more gradual boattail to the lower half of the grain lobe would probably be much more effective but would lead to severe grain processing problems. The wake behind the grain lobes also carried over into the convergent entrance region of the nozzle causing circumferential variations in the nozzle Mach numbers. However, the results also indicated that the adverse induced effects were greatly diminished when the nozzle grain had regressed 34 percent.

Lewis Research Center,
National Aeronautics and Space Administration,
Cleveland, Ohio, February 20, 1967,
728-00-00-01-22.

REFERENCE

1. Salmi, Reino J.: Compressed-Air Model Investigation of Solid Rocket Overpressures Due to Interference from Aft-End Ignition Rocket. NASA TN D-3537, 1966.

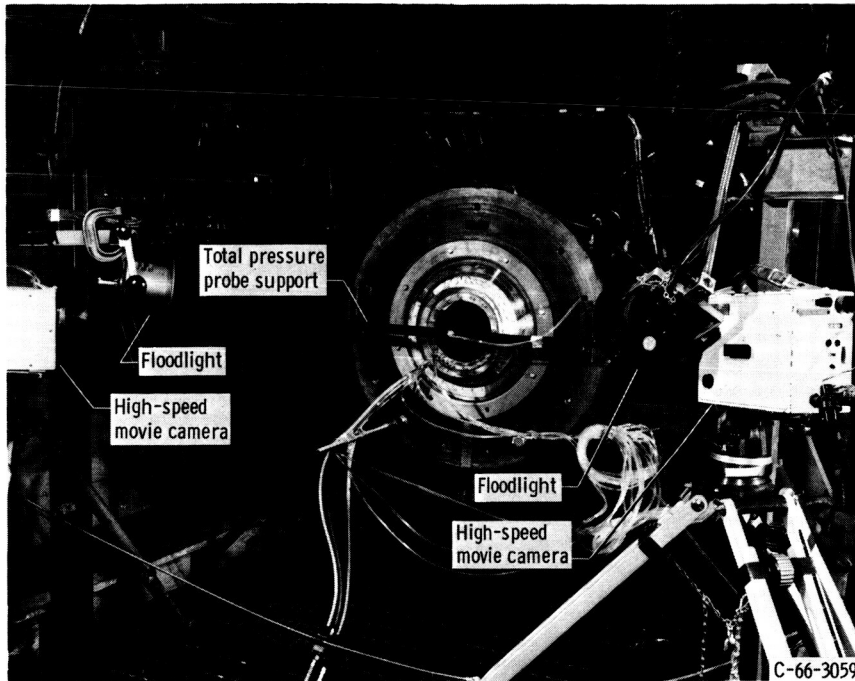
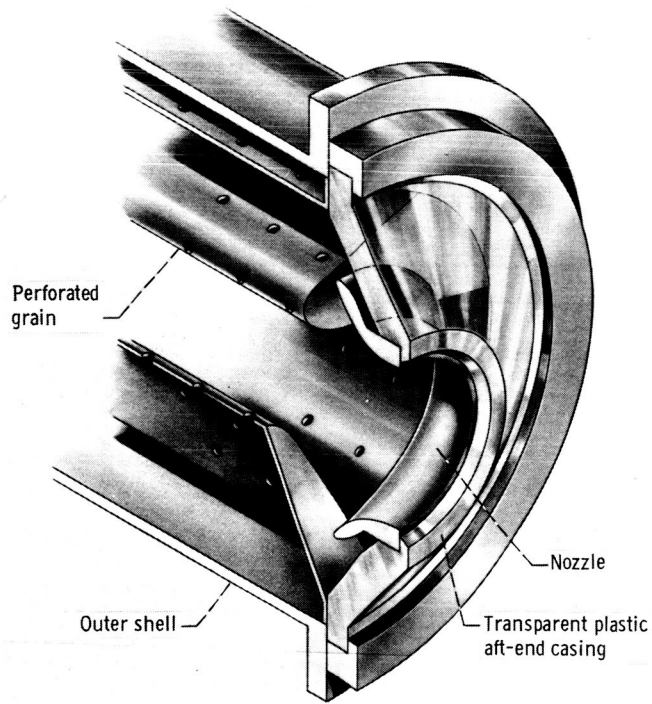
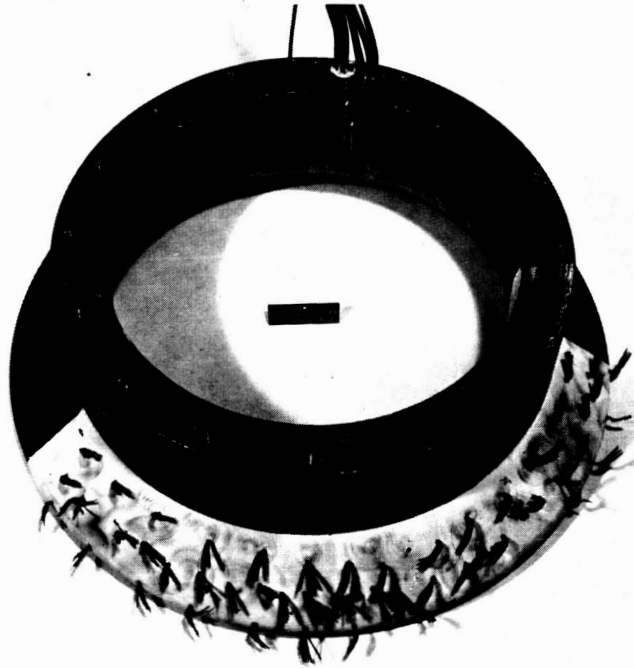


Figure 1. - 1/14.2-Scale model of 260-inch solid rocket with submerged nozzle in altitude test facility.



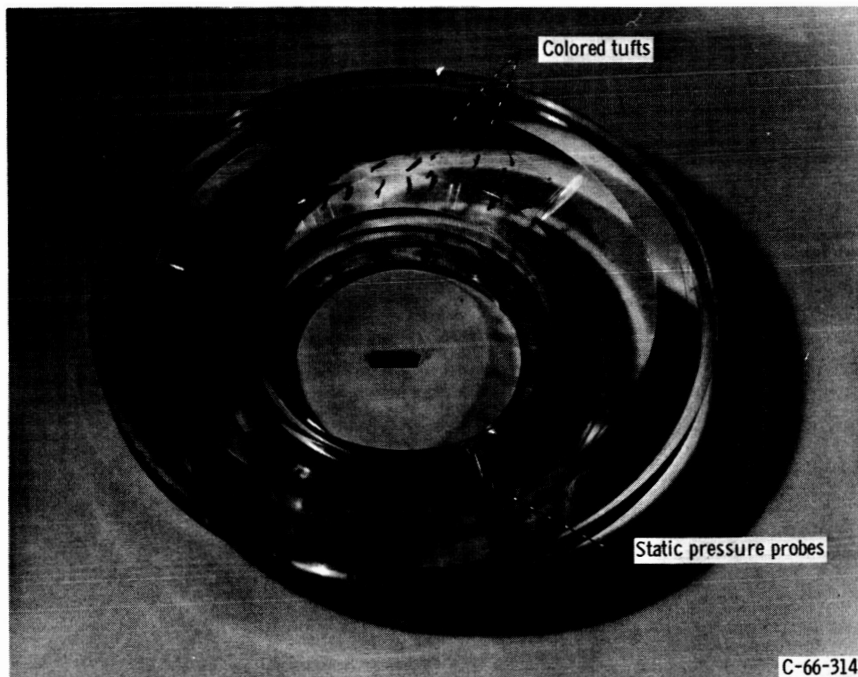
CD-8907

Figure 2. - Aft end of 1/14.2-scale model of 260-inch solid rocket with submerged nozzle.



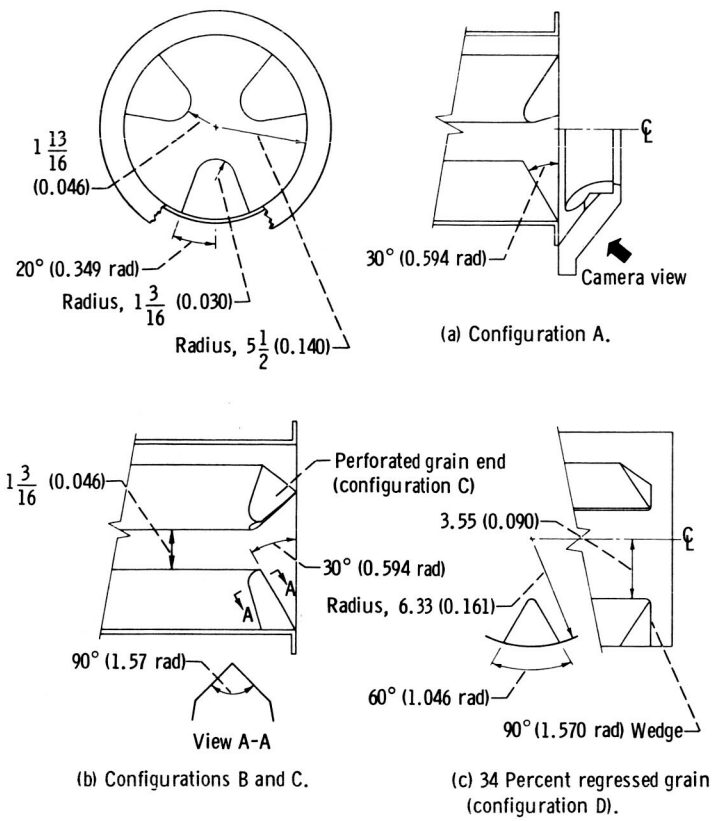
C-66-3139

Figure 3. - View of submerged nozzle showing underside of nozzle lip.



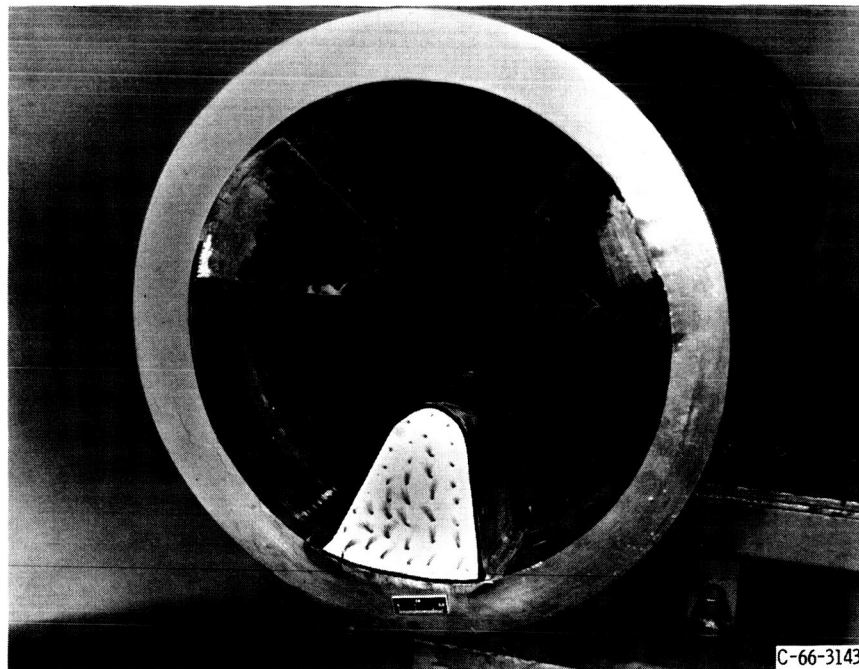
C-66-3141

Figure 4. - View of interior surface of transparent aft-end casing.



CD-8908

Figure 5. - Geometry of simulated propellant grain configurations. (Linear dimensions in inches (meters).)



C-66-3143

Figure 6. - Simulated propellant grain, grain lobes with flat ends (configuration A).

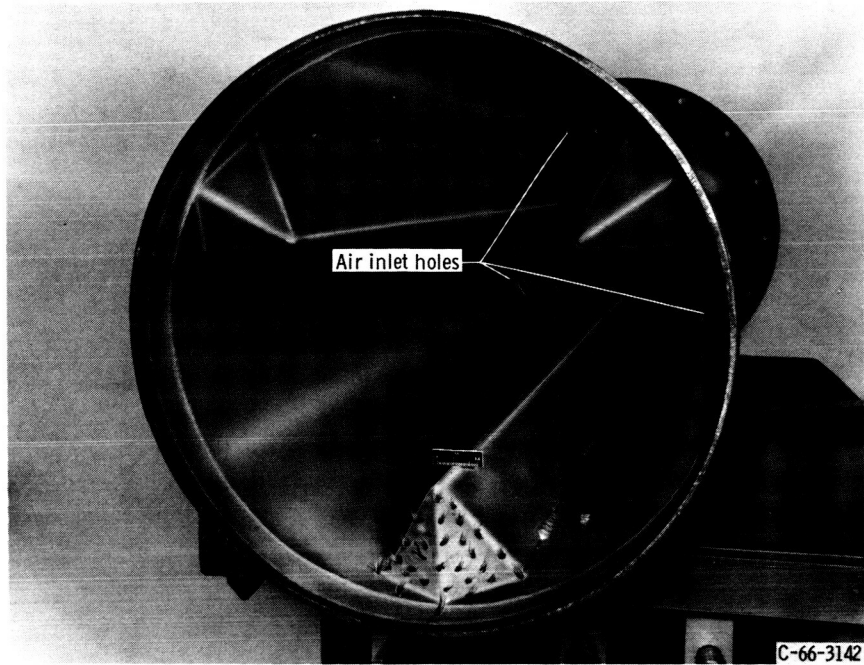


Figure 7. - Simulated 34 percent regressed grain (configuration D).

Static orifice	X		R	
	in.	m	in.	m
1	0.75	0.0101	3.21	0.0815
2	1.25	.0318	3.35	.0841
3	1.57	.0399	3.50	.0889
4	1.87	.0475	3.72	.0945
5	2.12	.0538	4.00	.1016
6	2.28	.0579	4.34	.1102
7	2.32	.0589	4.66	.1184
8	2.13	.0531	4.84	.1229
9	1.87	.0475	4.72	.1199
10	1.61	.0409	4.45	.1130
11	1.35	.0343	4.18	.1062
12	.91	.0231	4.17	.1059
13	2.92	.0742	5.72	.1452

Throat radius, 3.12 in. (0.0792 m).

Total probe	X		R	
	in.	m	in.	m
A	0	0	0	0
B	0	0	2.50	0.0635
C	0	0	2.98	.0757
D	1.11	0.0282	4.15	.1054
E	1.57	.0399	4.67	.1186

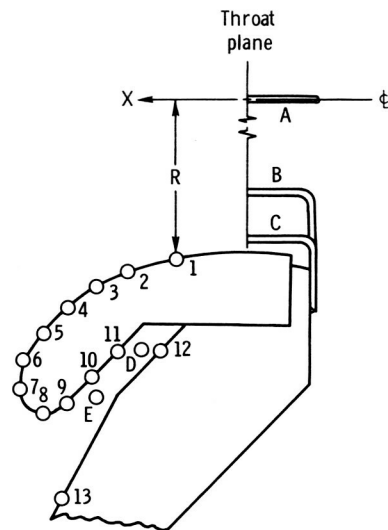
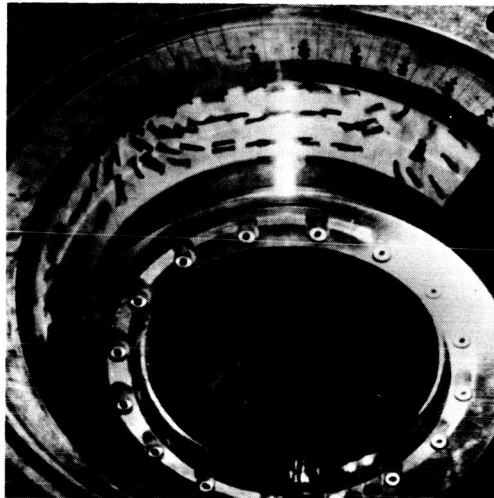


Figure 8. - Location of static and total pressure instrumentation.



(a) Configuration A.

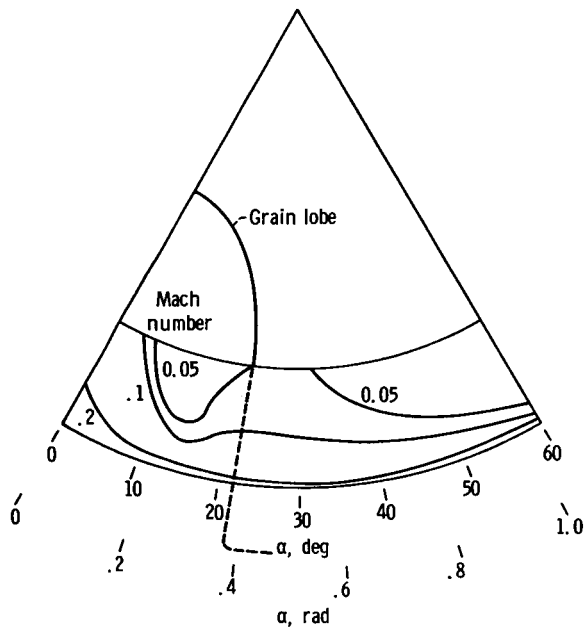


(b) Configuration B.

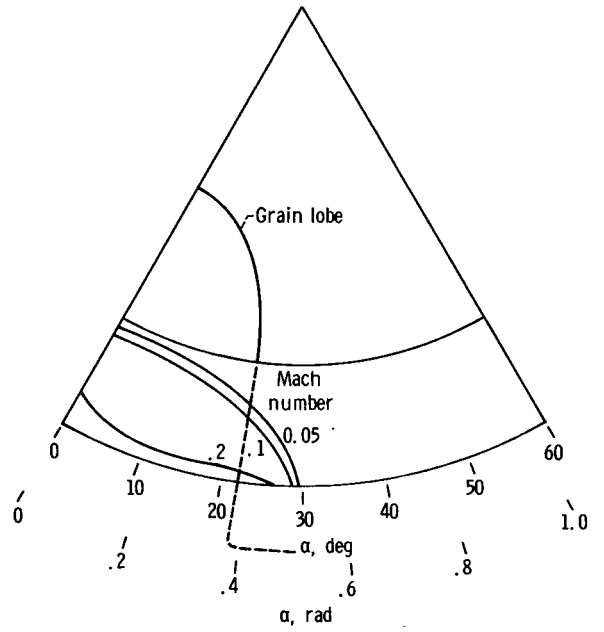


(c) Configuration D.

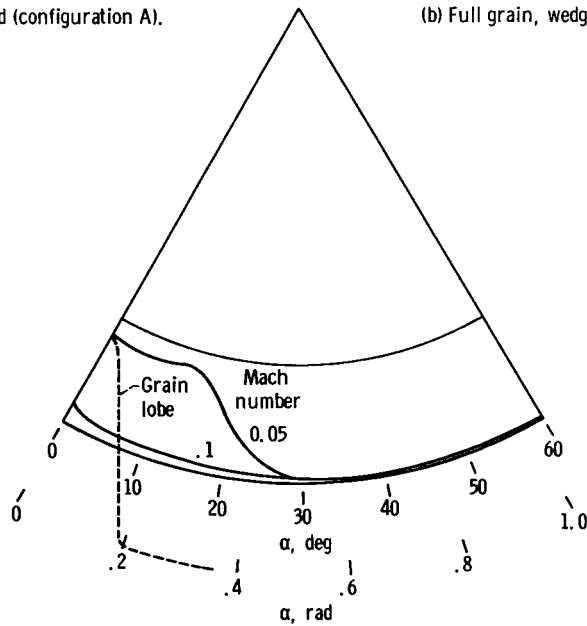
Figure 9. - Enlarged frames from high-speed movies of tufts in annular passage between nozzle lip and aft-end casing showing direction of airflow.



(a) Full grain, flat end (configuration A).

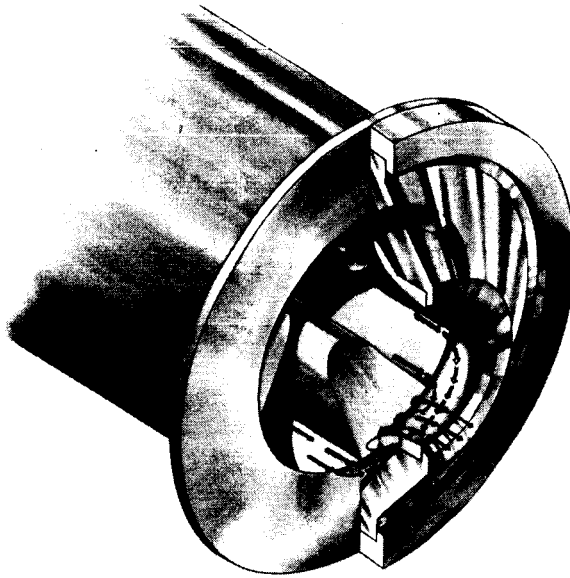


(b) Full grain, wedge end (configuration B).



(c) 34 Percent regressed grain (configuration D).

Figure 10. - Mach number contours in annular passage between nozzle lip and aft-end casing.



CD-8906

Figure 11. - Typical airflow pattern in annular passage between nozzle lip and aft-end casing.

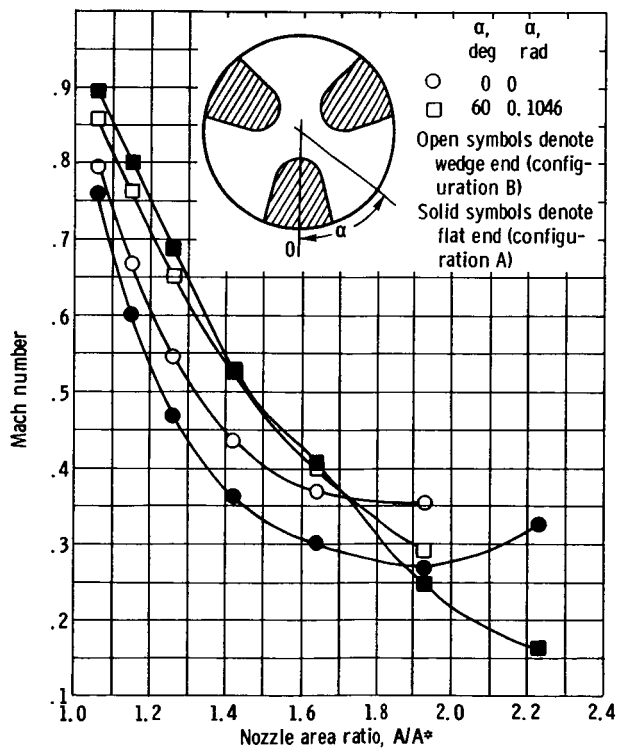


Figure 12. - Variation of nozzle Mach number at stations directly behind grain lobe and midway between grain lobes for flat and wedge end grain configurations.

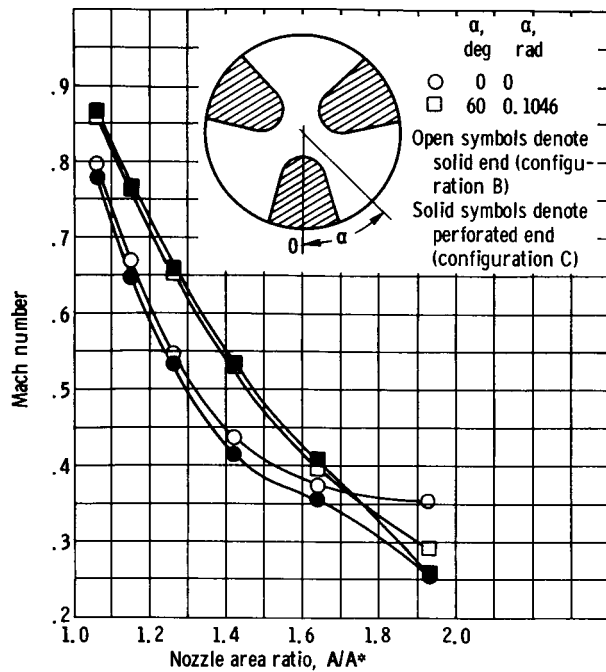


Figure 13. - Nozzle Mach number variation for wedge grain end configuration with and without grain end air bleed.

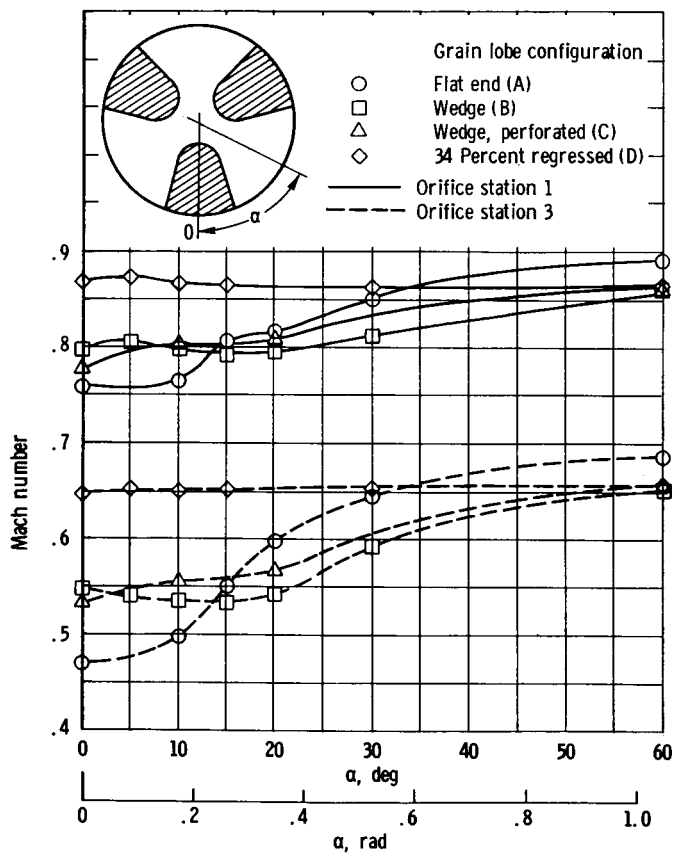


Figure 14. - Circumferential variation of nozzle Mach number at nozzle stations 1 ($A/A^* = 1.06$) and 3 ($A/A^* = 1.26$).